

Multiplet Effects in the Electronic Correlation of One-Dimensional Magnetic Transition-Metal Oxides on Metals

J. Goikoetxea,¹ C. Friedrich,² G. Bihlmayer,² S. Blügel,² A. Arnau,^{1,3,4} and M. Blanco-Rey^{3,4}

¹ *Centro de Física de Materiales CFM/MPC (CSIC-UPV/EHU),
Paseo Manuel de Lardizábal 5, 20018 Donostia-San Sebastián, Spain*

² *Peter Grünberg Institut and Institute for Advanced Simulation, Forschungszentrum Jülich and JARA, 52425 Jülich, Germany*

³ *Departamento de Polímeros y Materiales Avanzados: Física, Química y Tecnología,
Facultad de Química UPV/EHU, Apartado 1072, 20080 Donostia-San Sebastián, Spain*

⁴ *Donostia International Physics Center, Paseo Manuel de Lardizábal 4, 20018 Donostia-San Sebastián, Spain*

(Dated: February 23, 2022)

We use the constrained random phase approximation (cRPA) method to calculate the Hubbard U parameter in four one-dimensional magnetic transition metal atom oxides of composition XO_2 ($X = \text{Mn, Fe, Co, Ni}$) on Ir(100). In addition to the expected screening of the oxide, i.e., a significant reduction of the U value by the presence of the metal substrate, we find a strong dependence on the electronic configuration (multiplet) of the $X(d)$ orbital. Each particular electronic configuration attained by atom X is dictated by the O ligands, as well as by the charge transfer and hybridization with the Ir(100) substrate. We find that MnO_2 and NiO_2 chains exhibit two different screening regimes, while the case of CoO_2 is somewhere in between. The electronic structure of the MnO_2 chain remains almost unchanged upon adsorption. Therefore, in this regime, the additional screening is predominantly generated by the electrons of the neighboring metal surface atoms. The screening strength for $\text{NiO}_2/\text{Ir}(100)$ is found to depend on the $\text{Ni}(d)$ configuration in the adsorbed state. The case of FeO_2 shows an exceptional behavior, as it is the only insulating system in the absence of metallic substrate and, thus, it has the largest U value. However, this value is significantly reduced by the two mentioned screening effects after adsorption.

I. INTRODUCTION

The metallic or insulating character of a system often lies beyond the descriptive power of one-electron models. In systems with localized electrons, such as in d -electrons, the existence of a gap is determined by three quantities: (i) the charge transfer (CT) gap Δ_{Ld} from a ligand (L) to the open d shell, (ii) the bandwidth that results from hybridization, and (iii) the d -orbital intrashell electron-electron Coulomb interaction, usually expressed in terms of correlation U and exchange J parameters. The renowned Zaanen-Sawatzky-Allen (ZSA) diagram abridges the various insulating and metallic phases resulting from these interactions [1]. Samewise, exchange interactions between spin-polarized ions stem from the aforementioned terms of the Hubbard Hamiltonian, as a direct consequence of the competition between electron itinerance and intrashell Coulomb interaction. While the bare interaction amounts to a few tens of eV in $3d$ transition metals (TM), the effective interaction is strongly damped by the electronic screening. Therefore, its magnitude depends on the electronic structure of the particular system, e.g., on the hybridization of the d orbitals and charge transfer effects. It has been found that the effective interaction parameter is of a few eV in bulk oxides and, at the metal/oxide interface, the Coulomb interaction is further screened by twice the image charge formation potential [2, 3]. The dimensionality d determines the screening length: for $d \leq 2$, long-range screening is suppressed and anti-screening may exist at intermediate inter-atomic distances [4, 5].

Several electronic structure methods rely on realistic

effective U parameters to account for screening mechanisms as an alternative to more complex calculations. In this context, the popular LDA+ U [6] used in density functional theory (DFT) allows to include correlation effects via an orbital-dependent functional that is applied specifically to the localized orbitals. It can be formulated as a rotationally invariant functional dependent on constant U and J values [7]. In the next level of complexity we find many-body methods beyond the one-electron picture of DFT, for example, LDA++ [8], GW [9], MP2 [10] or RPA [11] and, notably, methods based on dynamical mean-field theory (DMFT) [12–14].

LDA+ U and DMFT-based methods require suitable U and J parameters to predict correlation-dependent properties. A number of methods have been proposed to determine those quantities self-consistently from first principles, such as constrained DFT [15, 16] (recently improved to avoid supercell calculations [17, 18]) and constrained random-phase approximation (cRPA) [19, 20]. The latter approach also gives access to the frequency dependence of the interaction. In it, the polarizability contribution of electrons in the correlated subspace is excluded to obtain a screened interaction \hat{U} , whose matrix elements in the localized basis are the sought-for $U_{mn,m'n'}$ Coulomb matrix elements of the Hubbard Hamiltonian, where indices label the orbitals. In practice, maximally localized Wannier functions (MLWF) are used as basis sets [21–24].

In this paper, we use cRPA to calculate \hat{U} in four one-dimensional magnetic transition-metal oxides (TMO) of composition XO_2 ($X = \text{Mn, Fe, Co, Ni}$) on Ir(100). In addition to the expected screening effect of the metal sub-

strate, we find a strong dependence of the U value on the electronic configuration (multiplet) of the $X(d)$ orbital. The particular configuration attained by X is dictated by the O ligands, as well as by the charge transfer and hybridization with the substrate. MnO_2 and NiO_2 chains represent two different regimes. The electronic structure of the MnO_2 chain remains almost unchanged upon adsorption. In this regime screening by the neighboring metal surface atoms applies. In contrast, NiO_2/Ir is in the other regime, where screening is dominated by the $\text{Ni}(d)$ configuration adopted in the adsorbed state. The cRPA calculations show that the multiplet effect cannot be uncoupled from screening by the metal.

XO_2 chains grown in ultra-high vacuum on $\text{Ir}(100)$ are aligned along the $[100]$ crystallographic direction and can reach lengths up to 130 nm [25]. The chains self-organize in a (3×1) missing-row superstructure (see Fig. 1(c)) with rotational domains of $\sim 100 \text{ nm}^2$ extension. Low-energy electron diffraction [LEED-I(V)] shows that the Ir atoms below the chain are lifted to leave room for the X atoms, which are not coplanar with the oxygens [25, 26]. $\text{Pt}(100)$ can serve as growth template as well [26, 27]. DFT+ U calculations in the literature have used a low value $U - J = 1.5 \text{ eV}$ for these systems on the premise that the interactions within the $X(d)$ orbital are heavily screened by the metal substrate [25, 27]. Weak antiferromagnetic (AFM) coupling is found along MnO_2 and CoO_2 on $\text{Ir}(100)$ [25] and CoO_2 on $\text{Rh}(553)$ [28], $\text{FeO}_2/\text{Ir}(100)$ is ferromagnetic (FM) and the Ni spin moment in $\text{NiO}_2/\text{Ir}(100)$ is quenched [25]. A long-range chiral non-collinear modulation is also observed along $\text{MnO}_2/\text{Pt}(100)$ using scanning tunneling microscopy [27]. Substrate-mediated RKKY exchange promotes additional lateral interactions between the $\text{MnO}_2/\text{Ir}(100)$ chains, which are also non-collinear and chiral [29]. The modelling of these magnetic properties is subject to understanding Coulomb interactions. As a matter of fact, a variation in the Curie and Néel critical temperatures has been observed during magnetic oxide film growth on metals that can be explained by the image potential screening length [30, 31]. As a first approximation, the magnetic exchange along the chain follows from the electron hopping through $X(d)$ - $\text{O}(p)$ - $X(d)$ orbitals (superexchange) [32, 33]. In the CT insulator limit ($U \gg \Delta_{pd}$) [1], the coupling constant of the AFM channel roughly scales as $\sim t^4/U^3$, where t accounts for the hopping integrals, and the FM one as $\sim -t^2/U$. Additionally, the four-fold coordination of $X(d)$ allows for competing hopping pathways that tend to weaken the magnetic interactions [28]. All in all, the combined effect of the $\text{O}(p)$ ligands and Ir substrate screening channels will lead to a system-dependent renormalization of intraorbital $X(d)$ interactions with consequences for the previously described magnetic properties. This understanding of system dependent interactions is the purpose of this study.

The paper is organized as follows: in Section II we describe the DFT and cRPA calculations; the results and

discussion are presented in Section III, which is divided into Subsections III A and III B on the isolated and the adsorbed chains on $\text{Ir}(100)$, respectively. Finally, conclusions are drawn in Section IV.

II. THEORETICAL METHODS

Ideal free-standing planar XO_2 chains are modelled in the supercell approach. The geometry is found by relaxing the X-X distances and X-O bonds in a calculation with the VASP code (projector augmented wave potentials and a plane-wave basis set [34, 35]) using the GGA+ U approximation [25, 29]. The details of the geometry determination are described in the Supplementary Material (SM) Tables S1 and S2. For the $\text{XO}_2/\text{Ir}(100)$ model structures (see Fig. 1(d)), a (3×1) missing-row reconstructed substrate with the experimental in-plane lattice constant $a = 2.71 \text{ \AA}$ is used, as found in the LEED-I(V) study of Ref. [25]. The substrate slab consists of five monolayers, where the bottom layer is kept fixed during the relaxation. Two layers are kept in the cRPA calculations [36]. These geometry relaxations have been carried out at a fixed value $U = 1.5 \text{ eV}$, used also in other works with supported XO_2 chains [25, 29]. In the coplanar isolated chains the equilibrium geometry shows low sensitivity to the U value, but the spin state can be altered by a change in U (see SM Fig. S1).

The one-electron wavefunctions used in the cRPA calculations are obtained from *ab-initio* DFT+ U calculations [6] with the generalized-gradient PBE functional [37] in the fully-localized limit [38] for the LDA+ U double-counting term. The used code, FLEUR [39], is based on the full-potential linearized augmented plane waves (FLAPW) formalism [40–42]. The local basis functions are expanded to $l_{max} = 8, 6$ and 8 inside the X, O and Ir muffin tin spheres, of radii 2.1, 1.2 and 2.4 a.u., respectively. The wavevector cut-off in the interstitial region is 5 a.u.^{-1} for wavefunctions and 14 a.u.^{-1} for the potential, using a $10 \times 3 \times 3$ Brillouin zone sampling (the sampling in the perpendicular direction is needed for constructing the Wannier functions). The Fermi level was determined by a Fermi-Dirac smearing of width 0.27 eV. To adapt these parameters to each particular case, slight modifications are performed that can be found in the SM Table S3.

For the unsupported XO_2 chains, MLWFs [21, 22] for 11 bands are constructed with projections of d type on $X=\text{Fe,Co,Ni}$ and s, p_x, p_z or $p = (p_x, p_y, p_z)$ orbitals on O. For MnO_2 , 13 bands are needed (d on Mn and s, p on O). In the supported case, the Wannier basis needs to be extended to include the Ir states, since the oxide states are strongly hybridized with the metal substrate. Up to 41 bands are considered, including p, d projections on X, s, p on O and sp^3d on Ir. The static partially screened Coulomb interaction matrices in the Wannier basis are calculated with the cRPA formalism as implemented in the code SPEX [43], where correlated subspaces

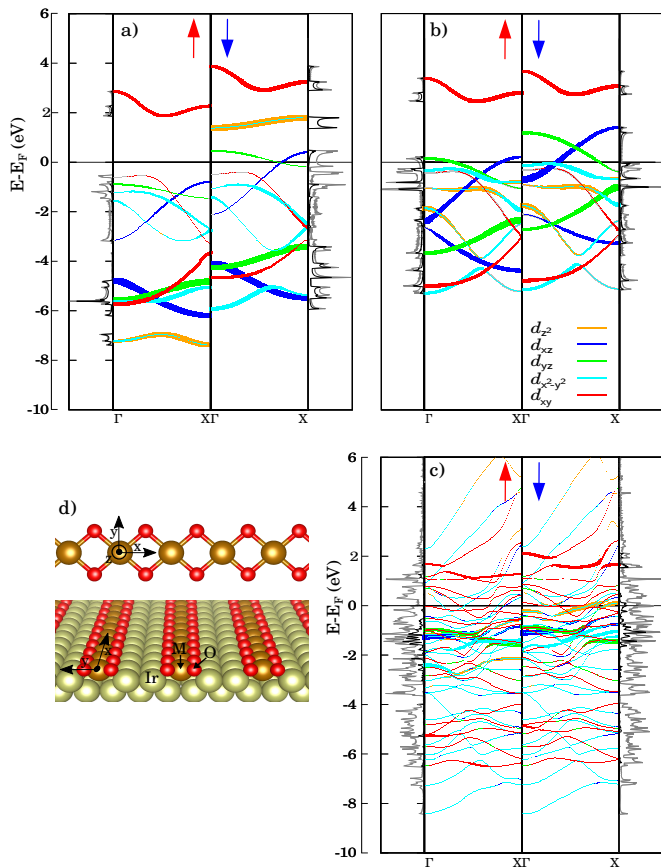


FIG. 1. Band structures (central subpanels) and densities of states (lateral subpanels) for NiO₂ chains, free-standing in the C1 (panel a) and C2 (b) configurations and supported on Ir(100) (c). Spin majority and minority contributions are indicated by red and blue arrows, respectively. The colour code indicates the Ni(*d*) orbital resolved bands, obtained from projection on the corresponding MLWFs, with dot sizes accounting for the magnitude of the projection. The full bands are shown as gray dotted curves for the isolated chains only. The solid gray and black curves are the total and Ni(*d*)-projected densities of states, respectively, in each system in arbitrary units (the gray curve in the bottom panel does include the Ir atoms contribution). The model (d) shows the atomic structure of the free-standing and adsorbed chains on the missing row (3 × 1) Ir(100) surface.

can be selected *ad hoc* to obtain information about different screening channels in the system. The effective parameters U, J are obtained by averaging the Coulomb interaction matrix elements as described in Ref. [38].

In cRPA, the Hilbert space is divided into the correlated (*d*) and the remainder (*r*) parts. The two subspaces are orthogonal. The total polarization is $\hat{P} = \hat{P}_d + \hat{P}_r$, where \hat{P}_d contains $d \rightarrow d$ transitions only, while \hat{P}_r accounts for $d \rightarrow r, r \rightarrow d$ and $r \rightarrow r$ transitions. The fundamental equations of the cRPA formalism [19] are (dropping the frequency dependence) $\hat{W} = (1 - \hat{W}_r \hat{P}_d)^{-1} \hat{W}_r$ and $\hat{W}_r = (1 - \hat{v} \hat{P}_r)^{-1} \hat{v}$, where \hat{v}, \hat{W}_r and \hat{W} are the bare, effective and fully-screened

Coulomb interactions, respectively. The spherical average of the static limit of \hat{W}_r is the sought-for Hubbard U parameter. The use of MLWFs basis to isolate the localized states belonging to the *d* subspace is commonplace and there are different methods to uncouple the *r* and *d* subspaces [23]. Here, we use the one described in Ref. [24], which is fully basis-set-independent. In it, the transitions are weighted by the probability that the initial and final states belong to the *d* subspace. Finally, the effective Coulomb interaction matrix elements $U_{mn,m'n'}$ are calculated for a selected subset of functions out of the whole Wannier set. In order to interpret the $U_{mn,m'n'}$ matrix elements obtained in this cRPA approach as atomic Coulomb integrals, we make sure that the MLWFs conserve the symmetry of the atomic orbitals. The MLWFs are also used to calculate band structure projections and orbital occupancies.

III. RESULTS AND DISCUSSION

A. Isolated planar XO₂ chains

In this subsection, we study an ideal situation where the main substrate effects are suppressed, namely the geometry change (the here-assumed coplanarity between the X and O atoms is lost in the adsorbed geometry) and charge redistribution at the metal-oxide interface. These idealized planar chains allow us to examine the screening originated exclusively by the X-O bond formation and the one-dimensionality of the system.

All the cRPA calculations are initialized with the electronic structures obtained with $U_0 = 5.5$ eV and $J_0 = 0$. Once the first U_1 is calculated using cRPA, a new DFT+ U cycle is started with this value. After 4-5 iterations, convergence is achieved for MnO₂, FeO₂ and CoO₂. The resulting U and J values for the $\uparrow\uparrow$ spin channel, shown in Table I, lie in the 5-7 eV range and are obtained independently of the U value used in the initial iteration (this was checked by starting from $U_0 = 3.5$ and 7.5 eV). The effective parameter U plays the role of the F^0 Slater integral in the Coulomb interaction term and the effective intra-atomic exchange parameter is $J = (F^2 + F^4)/14$ in the case of a *d*-orbital [38]. F^2 and F^4 are known to be almost insensitive to screening effects [3, 44] and, in fact, we obtain the typical value $J \simeq 1$ eV in the cRPA calculations. Due to the spin dependence of the single-particle states, the Wannier functions exhibit a spin dependence, too. As a consequence, we can distinguish between the matrix elements $U^{\uparrow\uparrow}, U^{\uparrow\downarrow}$, and $U^{\downarrow\downarrow}$. They exhibit a spread of ≈ 0.5 eV about their average values for FeO₂ and MnO₂, and of ≈ 0.2 eV for NiO₂ and CoO₂ (see SM Table S5). Spreads in the J values are ≤ 0.2 eV.

The case for NiO₂ deserves further attention. Unlike in the other chains, two electronic configurations of the Ni(*d*) orbital are stabilized in the initial run for different U_0 values, labelled C1 and C2 hereafter. The C1 and C2 configurations are preserved throughout the sub-

TABLE I. Converged values of U and J , averaged over the $\uparrow\uparrow$ spin channel orbitals, for the transition metal atoms in free-standing planar and Ir-supported XO_2 chains. \tilde{U} are the values calculated in the shell folding approach [45]. All units in eV.

XO_2	U	J	\tilde{U}	XO_2/Ir	U	J
Ni (C1)	6.59	1.17	8.45	Ni	1.71	0.87
Ni (C2)	2.41	1.01	7.03			
Mn	6.21	1.04	6.57	Mn	3.78	0.98
Co	5.73	1.11	8.62	Co	2.39	0.90
Fe	7.67	1.13	9.06	Fe	1.38	0.80

TABLE II. d -orbital occupancies and magnetic spin moments of the Ni atom at free-standing (C1 and C2 configurations) and Ir-supported NiO_2 .

	Spin	d_{z^2}	d_{xz}	d_{yz}	$d_{x^2-y^2}$	d_{xy}	$\mu_{\text{Ni}} (\mu_B)$
NiO_2 : C1	\uparrow	0.99	0.99	0.99	0.99	0.54	1.23
	\downarrow	0.03	0.94	0.85	0.97	0.42	
NiO_2 : C2	\uparrow	0.99	0.91	0.86	0.99	0.48	0.55
	\downarrow	0.99	0.64	0.61	0.99	0.46	
NiO_2/Ir	\uparrow	0.97	0.95	0.95	0.97	0.62	0.52
	\downarrow	0.59	0.94	0.95	0.96	0.41	

sequent cRPA cycles, which converge to two different U values (see Table I). DFT+ U calculations with $U_0 < 4$ eV yield C2 as the most stable configuration and finally $U = 2.41$ eV, while C1 is the preferred configuration for $U_0 \geq 4$ eV, leading to $U = 6.59$ eV. The details of d -orbital occupancies that define C1 and C2 are gathered in Table II for the DFT+ U calculations at the converged U values. Occupancies are calculated as integrals of the projected densities of states (PDOS) on the individual d -like MLWFs (see SM Fig. S3). The projected band structure is shown in Fig. 1.

The Ni spin moments obtained for the C1 and C2 configurations, 1.23 and 0.55 μ_B , deviate from an integer value. The closest integer is 1 μ_B in both cases, which leads us to interpret C1 and C2 to be two Ni multiplets of the same *nominal* spin state $S = 1/2$. The bare Coulomb parameters in the C1 and C2 configurations take essentially similar values, differences between individual matrix elements being, on average, 8%. This small difference in the bare Coulomb matrix is solely due to differences in the Wannier functions shape. Indeed, their real-space representations show marginal differences (see SM Fig. S7). Therefore, the Wannier functions' shape cannot be responsible for the different U values found for C1 and C2. Instead, the origin must be in the electronic configurations adopted by Ni(d) upon the formation of the oxide chain. To confirm this interpretation, we have analyzed the bare and screened Coulomb matrix elements obtained in cRPA calculations with different choices of the constrained subspace. The $\uparrow\uparrow$ spin channel values of the ele-

ments needed in the determination of U , i.e. $U_{mn,mn}$, are summarized graphically in Fig. 2 with the contracted index notation U_{mn} . Using as baseline wavefunctions those of the C1 and C2 states at the previously converged U values [panels (a,d)], the new U_{mn} have been calculated with subspaces that include also the O(s) [panels (b,e)] and O(p) orbitals [panels (c,f)]. This means that in panels (a,d) the screening is (predominantly) due to O(sp), in panels (b,e) to O(p) and in panels (c,f) only to O(s). As a reference, the bare Coulomb matrix elements are shown in panel (g). The general trend is that the formation of Ni-O bonds largely screens the atomic Coulomb interaction at the Ni(d) orbital, reducing it from values ~ 25 to ~ 6.5 eV in C1 and to ~ 2.5 eV in C2. The comparison of data columns (a) *vs.* (b) and (d) *vs.* (e) in Fig. 2 shows that, for both configurations, the screening contribution of the O(p) electrons apparently suffices to reproduce the complete screening. This does not mean that there is no significant O(s) contribution, though. In panels (c,f) we see that the U value for d electrons [$\hat{U}(d,d)$] is screened by O(s) electrons from 25 to 15 eV and to 10 eV in C1 and C2, respectively. We draw two conclusions from this result: (i) the Coulomb screening of s and p channels on Ni(d) is not additive and (ii) the p screening is felt differently in C1 and C2 because each multiplet binds differently to the neighboring O atoms.

The DOS at the Fermi level $\rho(\epsilon_F)$ is usually taken as an indicator of the correlation strength. As a rule of thumb, the higher the DOS, the stronger the screening. Unlike in C2, in the C1 configuration the Fermi level lies in a spin-majority bandgap, i.e., C1 is a half-metal, which is consistent with a larger effective U value (note also that the ZSA theory allows for non-insulating behavior despite U being large [1]). This qualitative DOS difference is also manifested in the spin dependence of the interaction screening: the U parameters of metallic C2 show an almost negligible spin dependence, in contrast to the other half-metallic and insulating chains (see the comparison in the SM Table S5). As shown in Fig. 1, the main contribution to $\rho(\epsilon_F)$ has O(p) and partial d_{yz} character, which indicates conduction along a π band. In C1 and C2 the d_{xy} band is localized in energy and split across the Fermi level in a similar manner. The main difference between the two configurations is in the d_{z^2,x^2-y^2} band [46], which is partially filled and strongly hybridized with the O(p) in C1, while it is fully filled and localized in C2 (as it is partially filled in the C1 spin minority channel, it results in the different net spin moments of C1 and C2 configurations, as shown in Table II). This relates to the aforementioned conclusion point (ii) in the interpretation of the screening channels. Indeed, the bindings to the ligand differ qualitatively: the sharp peaks in the DOS around $E_F - 1$ eV form a $d-d$ gap for C2, in contrast to the $d-p$ gap of C1 (see Fig. 1 and SM Fig. S3), which suggests that the C2 configuration is prone to undergo a Mott transition [1].

The existence of high- U (C1) and low- U (C2) regimes can be rationalized by the estimates of the correlation

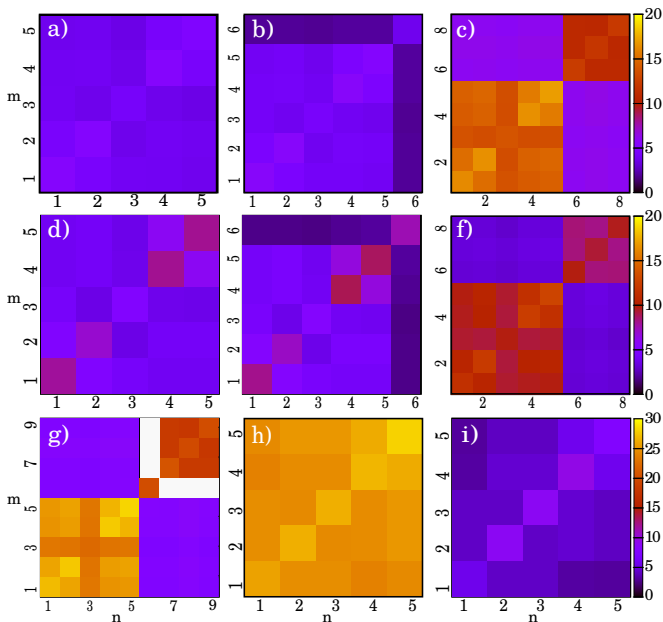


FIG. 2. Screened Coulomb matrix elements U_{mn} (\uparrow spin channel) in eV for the NiO_2 chain for selected orbitals screened by the remaining electrons. For the free-standing C1 configuration, the selection is: (a) d (indices ordered as $1 - d_{z^2}$, $2 - d_{xz}$, $3 - d_{yz}$, $4 - d_{x^2-y^2}$ and $5 - d_{xy}$), (b) d and $\text{O}(s)$ (index 6) and (c) d and $\text{O}(p)$ orbitals (indices ordered as $6 - p_z$, $7 - p_x$ and $8 - p_y$). (d-e) shows the same information as (a-c) but for the free-standing C2 configuration. In the bottom row, bare Coulomb matrix elements of (g) free-standing C1 and (h) Ir-supported NiO_2 , which we take as reference values. (i) For Ir-supported NiO_2 , U_{mn} elements of the d orbital screened by the rest of electrons. Note the different color scale for the panels (g) to (i)

energy at the $\text{Ni}(d)$ orbitals. These can be expressed as $E_U = U \sum_i n_i^\uparrow n_i^\downarrow$, where the n_i^σ are taken from the individual d -orbital occupancies of Table II. Owing to the aforementioned symmetry argument [46], we have considered d_{z^2, x^2-y^2} as an individual orbital with doubled maximum occupancy in the n_i^σ integrals shown in Table III. This simple argument provides the correct tendency obtained by cRPA for C1 and C2: the larger occupancy factor of C2 as compared to C1 suggests that the C2 is compatible with a smaller U value than C1. The E_U values themselves, namely 25.8 eV for C1 and 12.2 eV for C2, are very different. These energy estimates cannot be used to tell which configuration is more stable, as DFT+ U total energies obtained with different U values cannot be directly compared [47].

The results of Table I follow the trend laid down by the DOS at the Fermi level, shown in Fig. 3 and SM Fig. S4 for the other studied isolated chains: FeO_2 is insulating (its band structure shows the features of a conventional CT insulator) and, thus, screening is the weakest ($U = 7.67$ eV) among the different studied systems, while it is somewhat stronger in the half-metallic systems MnO_2 , CoO_2 and NiO_2 -C1 (with U values close to 6 eV),

TABLE III. $n^\uparrow n^\downarrow$ factors, correlation energy estimates E_U and spin moments of the transition metal atom in free-standing and supported chains.

	$n^\uparrow n^\downarrow$	E_U	μ_X (μ_B)
NiO_2 C1	3.98	26.2	1.23
NiO_2 C2	5.09	12.3	0.55
NiO_2/Ir	5.08	8.7	0.52
MnO_2	0.40	1.3	3.49
MnO_2/Ir	0.61	2.3	3.67
CoO_2	2.11	12.1	2.21
CoO_2/Ir	2.74	6.5	2.02
FeO_2	0.80	6.1	3.65
FeO_2/Ir	1.93	2.7	2.87

and even stronger in metallic NiO_2 -C2 ($U = 2.41$ eV). In Ref. [48] an expression of the screened U is given as the derivative of the Kohn-Sham potential with respect to the number n_d of electrons in the d orbital, which makes clear the explicit dependence on the relaxation of the d bands themselves for a given occupancy. When this expression is applied to the case of TM impurities of the same valence state embedded in an alkali metal (Rb), screening increases linearly with n_d , and it is stronger for monovalent than for divalent impurities. In the four XO_2 isolated chains this scaling does not apply, because of the more complex chemical environment, involving directional bonds and orbital-specific band dispersion. Indeed, while the d -shell occupancies are similar in the C1 and C2 configurations ($n_d(\text{C1}) = 7.71$ and $n_d(\text{C2}) = 7.92$), the U parameters are clearly different (Table I), due to the pronounced screening contribution from s and p electrons.

It has been argued in Ref. [45] that considering a correlated subspace of d -states in a system as the present chains, where the TM d orbitals strongly hybridize with the $\text{O}(p)$ ligands, often leads to an underestimation of the U values. In these chains, a bonding-antibonding $d_{xy} - p_{x,y}$ pair is formed, which appears as a one-dimensional dispersive occupied band of width ~ 2 eV (see red lines in Figs. 1 and 3). It is also manifested in the MLWF corresponding to the d_{xy} orbital, which acquires a nodal feature between the atoms (see the FeO_2 and NiO_2 cases in the SM Figs. S8 and S7, respectively). In principle, by having this localized wavefunction in the correlated space for cRPA, the splitting between the $X(d)$ space and the rest retains a partial contribution of the $\text{O}(p)$ ligands in the correlated subspace [23]. Alternatively, when treating p and d electrons as correlated, like in Fig. 2(c,f), the off-diagonal blocks $\hat{U}(d,p)$ account for intershell interactions that renormalize the intrashell interactions $\hat{U}(d,d)$ and $\hat{U}(p,p)$. This is the so-called "shell-folding" approach [45], whereby, if the total occupation of the d and p subspaces remains invariant under changes in U , the renormalization is written simply as

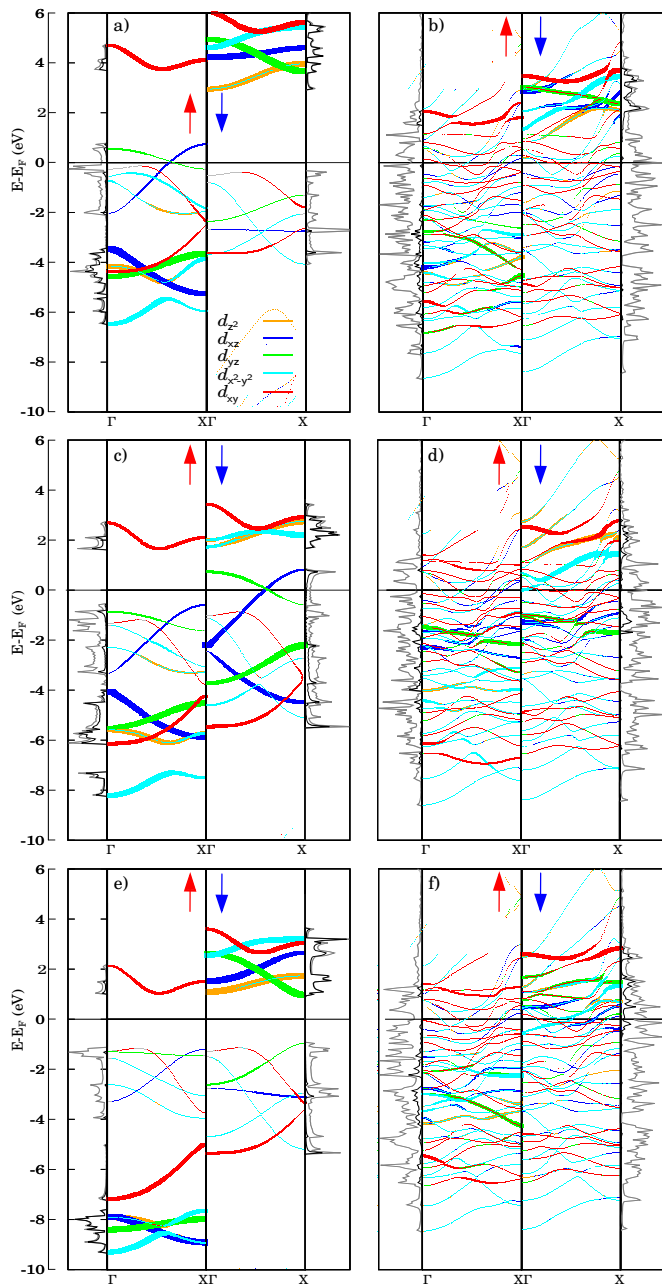


FIG. 3. The same information as in Fig. 1 is provided here for free-standing planar (left panels) and supported (right panels) XO_2 chains with $X = \text{Mn}$ (a,b), Co (c,d) and Fe (e,f).

$\hat{U}(d, d) = \hat{U}(d, d) - \hat{U}(d, p)$. This expression corrects the contribution of itinerant electrons to screening. With this approach we obtain $\tilde{U} > U$ (see Table I and further details in SM Table S6 and Figs. S6). In the case of MnO_2 the difference is only 0.36 eV, which means that the ligand is almost fully disentangled from the correlated d subspace (Fig. 4(a,b) shows the U_{mn} matrix elements), while for $\text{NiO}_2\text{-C2}$ the difference is as large as 4.62 eV. Moreover, we find an average $U(d, p) = 3.29$ eV in $\text{NiO}_2\text{-C2}$, while it is ~ 6 eV for the other four cases. We can

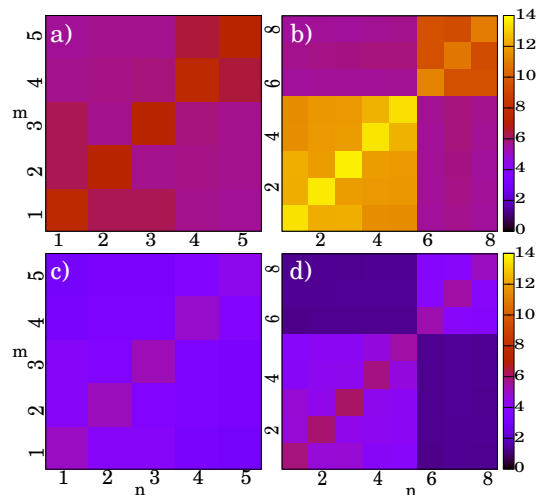


FIG. 4. Effective U_{mn} Coulomb matrix elements (in eV) in the isolated MnO_2 chain including (a) only $\text{Mn}(d)$ electrons and (b) $\text{Mn}(d)$ and $\text{O}(p)$ electrons in the correlated subspace. Panels (c,d): same quantities for the supported MnO_2 chain (Note, $\text{O}(s)$ electrons, which belong to the correlated space in panel (d), are not shown).

interpret this as the intershell interactions playing a distinct role in the screening in the C2 configuration.

B. $\text{XO}_2/\text{Ir}(100)\text{-}1 \times 3$

For oxide films on a metal, the Coulomb interaction can be modelled as the difference between the ionization and affinity energies, each corrected by the image potential energy E_{im} created by the charged $X(d)$ shell [2, 3], $U = E(d^{n-1}) + E(d^{n+1}) - 2E(d^n) - 2E_{im}$, where each total energy term is calculated for a fixed population of the d orbital. When the XO_2 chains are adsorbed on the $\text{Ir}(100)$ substrate there is, indeed, a reduction in the screened U values with respect to the planar free-standing chains in the range 0.7 – 6.3 eV, being strongest for FeO_2 . These results, obtained after 3-4 convergence cycles with cRPA, are shown in Table I. Figs. 1 and 3 show that $\rho(\epsilon_F)$ is mainly formed by Ir bands, which is a signature of the screening effect of the substrate. Hybridization between chain orbitals and Ir states, clearly visible in the band structures, results in a non-uniform charge redistribution at the interface. The reduction of the intraatomic Coulomb interaction in $X(d)$ will depend on the interfacial electronic structure details, which can be captured by *ab initio* methods, but not by an image charge model potential [49]. Charge transfer upon adsorption modifies the $X(d)$ orbital occupancies, eventually forcing it to adopt a very different multiplet configuration from that of the isolated case. As we have seen in the previous section, this can have a dramatic effect on the screening contribution of the p ligands. In brief, the overall screening observed upon adsorption may have a non-negligible indirect contribution from a mul-

triplet change. The importance of this additional mechanism depends on the chain composition. We note in passing that the non-coplanar atomic geometry adopted on the Ir(100) substrate alters the bandstructure of the chains, but this does not suffice to produce significant variations in the U, J values with respect to the planar geometry (we have checked that the U values obtained by cRPA for buckled MnO_2 free-standing chains, where the atomic positions are set as in the adsorbed geometry, are not significantly affected by this distortion, although it does change the bands dispersion, as shown in the SM Fig. S2).

We start by describing the case of Mn and Co oxide chains, as they share some common features. The substrate modifies the Mn and Co d -band energies by hybridization, causing in turn the filling of the partially occupied $d_{xz, yz\downarrow}$ bands and a subtle accumulation of $d_{xy\uparrow}$ states at the Fermi level (see Fig. 3). In the Co case, there is also an additional partial filling of $d_{x^2-y^2\downarrow}$ states (see SM Table S4). The $n^\uparrow n^\downarrow$ factors for the Mn(d) and Co(d) orbitals undergo a weak increase, compatible with a drop in the U value, as shown in Table III. Although the X(d) electronic configuration changes during adsorption are subtle, the interplay of the above-mentioned indirect mechanism, driven by the concomitant changes in the ligand effects, cannot be ruled out until the many-body interactions are examined. Here, an analysis of the selective inclusion of screening channels and shell-folding can be helpful. Fig. 4 shows that, in the $\text{MnO}_2/\text{Ir}(100)$ case, the screening by Ir atoms only (panel d) yields an intra-Mn(d) average interaction $U^{\text{Ir}}(d, d) = 4.66$ eV. This value is then renormalized by interaction with O(p) orbitals to $\tilde{U}^{\text{Ir}} = 3.29$ eV, which is close to the value $U = 3.78$ eV obtained by the regular method (panel c). This implies that for the adsorbed MnO_2 , as in the isolated case, the ligand orbitals are well disentangled and the screening by the Ir substrate causes the interaction to be further reduced by $\simeq 1$ eV. This estimation is obtained as $U^{\text{Ir}}(d, d) - U = 0.88$ eV or $U^{\text{Ir}}(d, d) - \tilde{U}^{\text{Ir}} = 1.37$ eV.

Next, we consider the Ni oxide chains. In the adsorbed state, the Ni(d) configuration resembles better that of C2 than C1 (see Tables II and III, and Fig. 2). Since the C1 configuration is not found on the surface (not even as a metastable state), we interpret this fact as a consequence of the multiplet effect playing a dominant role in the screening of Coulomb interactions in $\text{NiO}_2/\text{Ir}(100)$, leading to the low value of $U = 1.71$ eV (calculated for the $\uparrow\uparrow$ channel). Indeed, to probe the robustness of the result on Ir, we have initialized the cRPA iterations with high and low U_0 values and Ni(d) frozen C1 and C2 configurations. In all cases, the calculation converges towards the U values and occupancies shown in Tables I and II. The common feature with Co and Mn is that the filling of $d_{xz, yz}$ bands in C2 is completed by charge transfer from the substrate, as shown by visual inspection of the band structure (Fig. 1). Ni(d) states remain overall as narrow bands around the Fermi level. In particular, the hybrid d_{z^2, x^2-y^2} states, which form a narrow band at $E_F - 1$ eV

in the isolated NiO_2 chain, become partially occupied by a relatively weak hybridization with Ir states and, therefore, screening is expected to be enhanced. All in all, the multiplet features that lead to the low $U = 2.41$ eV value in isolated NiO_2 -C2 are present also in the $\text{NiO}_2/\text{Ir}(100)$ adsorbed case. The further reduction to $U = 1.71$ eV is compatible with the already mentioned hybridization mechanism, consisting of a reduction of $\simeq 0.9$ eV, as estimated from the $\text{MnO}_2/\text{Ir}(100)$ case. The same calculation for $\text{NiO}_2/\text{Ir}(100)$, shown in Table S6, yields a smaller reduction of $U^{\text{Ir}}(d, d) - U = 0.28$ eV, probably due to the stronger entanglement with O(p) ligands detected at NiO_2 -C2.

Finally, we address the FeO_2 case. A very efficient overall screening, with a dramatic reduction of the U value from 7.67 to 1.38 eV, is found in adsorbed $\text{FeO}_2/\text{Ir}(100)$. The Fe(d) multiplet is changed by interaction with the Ir substrate, changing from a $S = 2$ to a $S = 3/2$ state (see Table I). This is also reflected in the increase by one unit in the $n^\uparrow n^\downarrow$ factor. The FeO_2 bandstructure, which is that of a CT insulator when the chain is isolated, becomes conducting upon hybridization with Ir, as the Fe(d) spin-minority band bottom edge is pinned to the Fermi level. We attribute the strong U reduction of the Fe(d) shell to this insulating-to-metallic transition. The pinning of the Fe(d_\downarrow) band at the Fermi level persists when high U values are used in the band structure calculation.

Surprisingly, the pinning also persists when the chain is artificially lifted from the substrate. To understand the evolution of the substrate screening length, we have carried out cRPA for structures with intermediate height $z_{\text{Fe}} = 2.5$ Å and two initial U_0 values to prevent stagnation at metastable states. Starting from both $U_0^f = 7.67$ eV (the converged free-standing value) and $U_0^s = 1.38$ eV (the converged supported value), the value is stabilized at $U_2^{f,s} \simeq 3.5$ eV after two iterations and a residual peak of chain states is still visible at the Fermi level. A height as large as $z_{\text{Fe}} = 4$ Å is needed for these residual states to vanish, as shown in SM Fig. S5(d) (the PDOS corresponding to some of those cases is shown in SM Fig. S5). However, at this distance, the U parameter does not stabilize at the value of the free-standing chain U_0^f , but reduces to $U_1^f = 6.13$ eV after one iteration. Starting from the adsorbed value U_0^s , it results in $U_1^s = 3.81$ eV. Therefore, despite the hybridization of the chain states with the surface is negligible at $z_{\text{Fe}} = 4$ Å, a non-negligible screening persists. This behavior is not necessarily unphysical. Nevertheless, in order to accurately describe the screening for far-lying chains, a different exchange and correlation (xc) functional would be needed. Note, the GGA, being a semilocal xc functional, works by error cancellation, providing a poorer description when low electron densities are involved in the interactions, failing to provide an accurate asymptotic $1/z$ behavior.

IV. CONCLUSIONS

In summary, we have performed a cRPA investigation of magnetic one-dimensional transition metal oxide XO_2 chains deposited on a Ir(100) surface aimed at understanding the screening of intraorbital Coulomb interactions in the $X(d)$ shell under the combined effect of low dimensionality, the ligand field and a neighboring metal.

Calculations for the isolated XO_2 chains show a strong dependence of the Hubbard U parameter on the X species, ranging from 2.4 to 7.7 eV. In each case, the U reflects the insulating or (half)metallic character of the chain. Importantly, we find low- U and high- U regimes in the case of NiO_2 associated to $d-d$ (Mott-Hubbard) or $p-d$ (charge transfer) gap types, respectively. The gap type is determined by the Ni(d) electronic configuration or multiplet. In the particular case of NiO_2 , multiplets with even the same orbital filling and same spin state (as it is the case of the C1 and C2 multiplets found in the present work) lead to different regimes. Due to the interaction with the O(p) ligands, the inclusion of O(p) electrons in the cRPA correlated subspace results in a different renormalization and higher values of the U parameter for each transition-metal species. The increase is smallest for MnO_2 and largest for the NiO_2 in the Mott-Hubbard-like multiplet.

Since the ligand field is weak for MnO_2 , this case allows us to establish that the U reduction by interaction with the metallic substrate is $\simeq 0.9$ eV and a much larger reduction comes from the change of the occupa-

tion of the d -states. In general, however, the contributions of substrate and ligand cannot be uncoupled. Adsorption drives the formation of interfacial states and charge transfer to the chain, which in turn can undergo an insulator-to-metal transition (such is the FeO_2 case, where the value of U is reduced by almost 6 eV) or have its multiplet configuration altered. The latter is the scenario for $\text{NiO}_2/\text{Ir}(100)$, where a low value $U = 1.71$ eV is obtained in part because the substrate adopts the Mott-Hubbard-like multiplet. Incidentally, the fine details of the band dispersion play a lesser role in the determination of the U parameter.

All in all, Coulomb interactions in a low-dimensional oxide by a neighboring metal cannot be described in simple terms by a charge screening model. Instead, the fine details of the hybrid oxide-metal electronic structure must be considered, as they also affect the renormalization of the interactions due to the O(p) ligands.

ACKNOWLEDGMENTS

Projects PID2019-103910GB-I00 funded by MCIN/AEI/10.13039/501100011033/; GIU18/138 by Universidad del País Vasco UPV/EHU; IT-1246-19 and IT-1260-19 by Gobierno Vasco. Computational resources were partially provided by the DIPC computing center. S.B. acknowledges funding from the Deutsche Forschungsgemeinschaft (DFG) through priority program SPP 2137 “Skyrmionics” (Project BL 444/16) and the Collaborative Research Centers SFB 1238 (Project C01).

-
- [1] J. Zaanen, G. A. Sawatzky, and J. W. Allen, *Phys. Rev. Lett.* **55**, 418 (1985).
 - [2] D. M. Duffy and A. M. Stoneham, *Journal of Physics C: Solid State Physics* **16**, 4087 (1983).
 - [3] S. Altieri, L. H. Tjeng, F. C. Voogt, T. Hibma, and G. A. Sawatzky, *Phys. Rev. B* **59**, R2517 (1999).
 - [4] J. van den Brink and G. A. Sawatzky, *Europhysics Letters (EPL)* **50**, 447 (2000).
 - [5] L. Peters, E. Şaşıoğlu, S. Rossen, C. Friedrich, S. Blügel, and M. I. Katsnelson, *Phys. Rev. B* **95**, 155119 (2017).
 - [6] V. I. Anisimov, F. Aryasetiawan, and A. I. Lichtenstein, *Journal of Physics: Condensed Matter* **9**, 767 (1997).
 - [7] A. I. Lichtenstein, V. I. Anisimov, and J. Zaanen, *Phys. Rev. B* **52**, R5467 (1995).
 - [8] A. I. Lichtenstein and M. I. Katsnelson, *Phys. Rev. B* **57**, 6884 (1998).
 - [9] L. Hedin, *Phys. Rev.* **139**, A796 (1965).
 - [10] C. Møller and M. S. Plesset, *Phys. Rev.* **46**, 618 (1934).
 - [11] D. Langreth and J. Perdew, *Solid State Communications* **17**, 1425 (1975).
 - [12] G. Kotliar, S. Y. Savrasov, K. Haule, V. S. Oudovenko, O. Parcollet, and C. A. Marianetti, *Rev. Mod. Phys.* **78**, 865 (2006).
 - [13] S. Biermann, *Journal of Physics: Condensed Matter* **26**, 173202 (2014).
 - [14] S. Biermann, F. Aryasetiawan, and A. Georges, *Phys. Rev. Lett.* **90**, 086402 (2003).
 - [15] P. H. Dederichs, S. Blügel, R. Zeller, and H. Akai, *Phys. Rev. Lett.* **53**, 2512 (1984).
 - [16] M. Cococcioni and S. de Gironcoli, *Phys. Rev. B* **71**, 035105 (2005).
 - [17] I. Timrov, N. Marzari, and M. Cococcioni, *Phys. Rev. B* **98**, 085127 (2018).
 - [18] I. Timrov, N. Marzari, and M. Cococcioni, *Phys. Rev. B* **103**, 045141 (2021).
 - [19] F. Aryasetiawan, M. Imada, A. Georges, G. Kotliar, S. Biermann, and A. I. Lichtenstein, *Phys. Rev. B* **70**, 195104 (2004).
 - [20] F. Aryasetiawan, K. Karlsson, O. Jepsen, and U. Schönberger, *Phys. Rev. B* **74**, 125106 (2006).
 - [21] G. Pizzi, V. Vitale, R. Arita, S. Blügel, F. Freimuth, G. Géranton, M. Gibertini, D. Gresch, C. Johnson, T. Koretsune, J. Ibañez-Azpiroz, H. Lee, J.-M. Lihm, D. Marchand, A. Marrazzo, Y. Mokrousov, J. I. Mustafa, Y. Nohara, Y. Nomura, L. Paulatto, S. Poncé, T. Ponweiser, J. Qiao, F. Thöle, S. S. Tsirkin, M. Wierzbowska, N. Marzari, D. Vanderbilt, I. Souza, A. A. Mostofi, and J. R. Yates, *Journal of Physics: Condensed Matter* **32**,

- 165902 (2020).
- [22] N. Marzari and D. Vanderbilt, Phys. Rev. B **56**, 12847 (1997).
- [23] T. Miyake, F. Aryasetiawan, and M. Imada, Phys. Rev. B **80**, 155134 (2009).
- [24] E. Şaşıoğlu, C. Friedrich, and S. Blügel, Phys. Rev. B **83**, 121101 (2011).
- [25] P. Ferstl, L. Hammer, C. Sobel, M. Gubo, K. Heinz, M. A. Schneider, F. Mittendorfer, and J. Redinger, Phys. Rev. Lett. **117**, 046101 (2016).
- [26] P. Ferstl, F. Mittendorfer, J. Redinger, M. A. Schneider, and L. Hammer, Phys. Rev. B **96**, 085407 (2017).
- [27] M. Schmitt, C. H. Park, P. Weber, A. Jäger, J. Kemmer, M. Vogt, and M. Bode, Phys. Rev. B **100**, 054431 (2019).
- [28] J. G. Korobova, I. A. Nikitina, D. I. Bazhanov, and P. Ruiz-Díaz, The Journal of Physical Chemistry C **124**, 26026 (2020), <https://doi.org/10.1021/acs.jpcc.0c07762>.
- [29] M. Schmitt, P. Moras, G. Bihlmayer, R. Cotsakis, M. Vogt, J. Kemmer, A. Belabbes, P. M. Sheverdyeva, A. K. Kundu, C. Carbone, S. Blügel, and M. Bode, NATURE COMMUNICATIONS **10**, 10.1038/s41467-019-10515-3 (2019).
- [30] S. G. Altendorf, A. Reisner, B. Tam, F. Meneghin, S. Wirth, and L. H. Tjeng, Phys. Rev. B **97**, 165422 (2018).
- [31] S. Barman, A. K. Kundu, and K. S. Menon, Journal of Magnetism and Magnetic Materials **515**, 167292 (2020).
- [32] J. B. Goodenough, Phys. Rev. **100**, 564 (1955).
- [33] J. Kanamori, Journal of Physics and Chemistry of Solids **10**, 87 (1959).
- [34] G. Kresse and J. Hafner, Phys. Rev. B **47**, 558 (1993).
- [35] G. Kresse and D. Joubert, Phys. Rev. B **59**, 1758 (1999).
- [36] Inclusion of a third Ir layer in a cRPA iteration changes the obtained U value for MnO_2/Ir by $\sim 10\%$.
- [37] J. P. Perdew, K. Burke, and M. Ernzerhof, Phys. Rev. Lett. **77**, 3865 (1996).
- [38] V. I. Anisimov, I. V. Solovyev, M. A. Korotin, M. T. Czyżyk, and G. A. Sawatzky, Phys. Rev. B **48**, 16929 (1993).
- [39] FLEUR site: <http://www.flapw.de>.
- [40] H. Krakauer, M. Posternak, and A. J. Freeman, Phys. Rev. B **19**, 1706 (1979).
- [41] E. Wimmer, H. Krakauer, M. Weinert, and A. J. Freeman, Phys. Rev. B **24**, 864 (1981).
- [42] A. B. Shick, A. I. Liechtenstein, and W. E. Pickett, Phys. Rev. B **60**, 10763 (1999).
- [43] C. Friedrich, S. Blügel, and A. Schindlmayr, Phys. Rev. B **81**, 125102 (2010).
- [44] D. van der Marel and G. A. Sawatzky, Phys. Rev. B **37**, 10674 (1988).
- [45] P. Seth, P. Hansmann, A. van Roekeghem, L. Vaugier, and S. Biermann, Phys. Rev. Lett. **119**, 056401 (2017).
- [46] Due to the chain symmetry, bands stemming from d_z^2 and $d_{x^2-y^2}$ atomic orbitals hybridize. In fact, as shown in Fig. 1, anticrossing features appear for bands with weight in the MLWFs corresponding to d_z^2 and $d_{x^2-y^2}$, while not on bands with d_{xz} , d_{yz} or d_{xy} character, as the latter belong to different symmetry representations.
- [47] Since in DFT+ U the Hubbard terms are applied to a subset of Kohn-Sham eigenstates, which have no physical meaning on their own, only total energies obtained in same- U calculations can be compared. For the particular values $U = 6$ and $J = 1$ eV for Ni(d), we find that C2 is metastable with an energy difference of 0.33 eV with respect to C1.
- [48] I. V. Solovyev and P. H. Dederichs, Phys. Rev. B **49**, 6736 (1994).
- [49] The image potential tail behaves as $-q/4(z - z_X)$, where q is the X(d) charge, z_X is the X atom adsorption height and z the vertical distance from the surface. However, the X atom is too close to the surface for that law to be applicable, since it is partially inserted in the trough of the Ir missing row (z_X values lie in the 0.7-1.25 Å range [25]).

**Supplemental Material for: “Multiplet Effects in the Electronic
Correlation of One-Dimensional Magnetic Transition-Metal
Oxides on Metals”**

J. Goikoetxea,¹ C. Friedrich,² G. Bihlmayer,² S.
Blügel,² A. Arnau,^{1,3,4} and M. Blanco-Rey^{3,4}

¹ *Centro de Física de Materiales CFM/MPC (CSIC-UPV/EHU),
Paseo Manuel de Lardizábal 5, 20018 Donostia-San Sebastián, Spain*

² *Peter Grünberg Institut and Institute for Advanced Simulation,
Forschungszentrum Jülich and JARA, 52425 Jülich, Germany*

³ *Departamento de Polímeros y Materiales Avanzados: Física, Química y Tecnología,
Facultad de Química UPV/EHU, Apartado 1072, 20080 Donostia-San Sebastián, Spain*

⁴ *Donostia International Physics Center, Paseo Manuel
de Lardizábal 4, 20018 Donostia-San Sebastián, Spain*

(Dated: February 23, 2022)

TABLE S1. **Relaxed isolated coplanar XO_2 structures.** Equilibrium geometries have been obtained with the code VASP, based in a plane-wave basis set and projector augmented wave potentials [1, 2]. These are DFT+ U calculations [3] with $U = 1.5$ eV and the generalized gradient approximation PBE of the exchange and correlation functional [4]. To model the isolated chains, supercells that leave a 10 \AA vacuum spacing between chains are used. The basis is constructed with a $10 \times 1 \times 1$ sampling of the first Brillouin zone and a cut-off of 450 eV. The convergence thresholds are 10^{-5} eV for the total energies and 0.01 eV \AA^{-1} for the forces on the ions. The values in the table are the interatomic distances found after relaxation of the XO_2 chains with the ideal coplanar geometry.

	MnO ₂	FeO ₂	CoO ₂	NiO ₂
$d_{\text{X-X}}$ (\AA)	2.75	2.71	2.65	2.70
$d_{\text{O-O}}$ (\AA)	2.43	2.43	2.41	2.35
$d_{\text{X-O}}$ (\AA)	1.87	1.73	1.79	1.79

TABLE S2. **Relaxed structures of $\text{XO}_2/\text{Ir}(100)$.** For the supported chains, the known (3×1) missing row reconstructed structure has been relaxed, using a Ir substrate of five atomic planes, where the two bottom Ir planes are kept fixed. The unit cell lateral size is fixed by the Ir(100) lattice constant (2.71 \AA), and the vacuum spacing between slab replicas is 10 \AA . The first Brillouin zone sampling is $10 \times 3 \times 1$. Calculation details are as in the caption of Table S1. The values in the table are the relaxed interatomic distances d , the heights of the X and O atoms z measured from the topmost Ir plane, and the Ir interplanar distances Δ_i (between the average z of atomic plane i and $i + 1$), ordered from the topmost plane. Individual Ir atom displacements, not shown in the table, are $\simeq 0.1 \text{ \AA}$ at the topmost plane and $\leq 0.05 \text{ \AA}$ at the second and third planes.

	MnO ₂	FeO ₂	CoO ₂	NiO ₂
$d_{\text{O-O}} (\text{\AA})$	2.62	2.63	2.64	2.65
$d_{\text{X-O}} (\text{\AA})$	1.90	1.90	1.96	1.85
$z_{\text{O}} (\text{\AA})$	1.39	1.31	1.34	1.32
$z_{\text{X}} (\text{\AA})$	1.12	1.89	0.17	1.19
$\Delta_1 (\text{\AA})$	1.84	1.84	1.84	1.87
$\Delta_2 (\text{\AA})$	1.99	1.99	1.99	1.98
$\Delta_3 (\text{\AA})$	1.84	1.84	1.84	1.84

TABLE S3. **FLAPW calculations parameters.** Parameters used in the DFT+ U FLAPW calculations [5–7] with the code FLEUR [8] in order to obtain the wavefunctions used as input for the cRPA calculations for the supported chains on Ir(100). In parenthesis, the parameters corresponding to isolated chain calculations. R_{MT} are the muffin-tin radii for the local basis functions at atoms X (transition metal (TM)), O and Ir, which are expanded up to $l_{max} = 8, 6$ and 6 angular momentum components, respectively (non-spherical potential components are expanded up to $l_{max} = 6, 4$ and 6 , respectively). The cutoffs for the basis functions and potential/density in the interstitial regions are given by E_c^{pot}/E_c^{wvf} , respectively. The Brillouin zone was sampled by a $12 \times 3 \times 1$ k -point grid.

	MnO ₂	FeO ₂	CoO ₂	NiO ₂
R_{MT}^X (a.u.)	2.24(2.16)	2.28(2.14)	2.23(2.11)	2.23(2.11)
R_{MT}^O (a.u.)	1.27(1.22)	1.29(1.21)	1.26(1.19)	1.26(1.19)
R_{MT}^{Ir} (a.u.)	2.45	2.35	2.37	2.34
E_c^{wvf} (a.u. ⁻¹)	4.7(4.9)	4.5(5.0)	4.7(5.0)	4.6(4.5)
E_c^{pot} (a.u. ⁻¹)	14.2(14.7)	13.8(14.9)	14.2(14.9)	14.1(13.0)

TABLE S4. *d*-orbital occupancies and magnetic spin moments of the X atom (X=Mn,Fe,Co). Occupations are calculated from integrals of the PDOS curves (see Fig. S4).

The spin moment μ_X is obtained from the charge inside the X muffin-tin spheres.

	Spin	d_{z^2}	d_{xz}	d_{yz}	$d_{x^2-y^2}$	d_{xy}	$\mu_X (\mu_B)$
MnO ₂	↑	0.94	0.91	0.86	0.99	0.41	3.49
	↓	0.01	0.10	0.08	0.09	0.28	
MnO ₂ /Ir	↑	0.96	0.98	0.98	0.99	0.41	3.66
	↓	0.08	0.08	0.08	0.09	0.23	
FeO ₂	↑	0.98	0.98	1.00	1.00	0.59	3.67
	↓	0.01	0.21	0.14	0.11	0.49	
FeO ₂ /Ir	↑	0.95	0.97	0.97	0.98	0.68	2.87
	↓	0.25	0.41	0.17	0.36	0.28	
CoO ₂	↑	0.97	1.00	1.00	0.96	0.52	2.21
	↓	0.00	0.84	0.75	0.14	0.46	
CoO ₂ /Ir	↑	0.97	0.96	0.96	0.98	0.70	2.02
	↓	0.08	0.93	0.94	0.29	0.31	

TABLE S5. **Spin channel effect on the U parameter.** Values of the U and J parameters calculated from averages over the $\uparrow\uparrow$, $\uparrow\downarrow$ and $\downarrow\downarrow$ spin channels. Note that the spread in values is only ≈ 0.5 eV. All values in eV. The last columns show, for the isolated chain cases, the dimensionless coefficients $\delta_U = \frac{2(U^{\uparrow\uparrow}-U^{\downarrow\downarrow})}{U^{\uparrow\uparrow}+U^{\downarrow\downarrow}}$ and $\delta_J = \frac{2(J^{\uparrow\uparrow}-J^{\downarrow\downarrow})}{J^{\uparrow\uparrow}+J^{\downarrow\downarrow}}$, which accounts for the relative variation in each case as a function of the spin. The labels indicate the character of the chain: HM = half-metallic, M = metallic, or I = insulator. Note that the smallest variation of U and J parameters occurs at the metallic NiO₂ (C2) chain.

	$U^{\uparrow\uparrow}$	$U^{\uparrow\downarrow}$	$U^{\downarrow\downarrow}$	$J^{\uparrow\uparrow}$	$J^{\uparrow\downarrow}$	$J^{\downarrow\downarrow}$	δ_U	δ_J	
MnO ₂	6.21	5.95	5.73	1.04	0.95	0.89	0.080	0.155	HM
MnO ₂ /Ir(100)	3.78	3.53	3.33	0.98	0.88	0.83			
FeO ₂	7.67	7.38	7.12	1.13	1.04	0.97	0.074	0.152	I
FeO ₂ /Ir	1.38	-	1.32	0.80	-	0.73			
CoO ₂	5.73	5.58	5.45	1.11	1.05	1.00	0.050	0.104	HM
CoO ₂ /Ir	2.39	-	-	0.90	-	-			
NiO ₂ (C1)	6.59	6.49	6.38	1.17	1.13	1.10	0.032	0.062	HM
NiO ₂ (C2)	2.41	2.40	2.39	1.01	1.00	1.00	0.008	0.001	M
NiO ₂ /Ir	1.71	-	1.70	0.87	-	0.86			

TABLE S6. **Shell-folding details.** Determination of the \tilde{U} parameter by the shell folding approximation [9] using cRPA calculations where the correlated subspace is formed by the $O(p)$ and $X(d)$ orbitals. The values in the table are averaged over the indicated orbitals (dd , dp or pp) for the spin channel $\uparrow\uparrow$. The last column shows the difference with respect to the U parameter obtained in the usual cRPA calculation, where only the d orbitals form the correlated subspace.

All values in eV.

	$U(d, d)$	$U(d, p)$	$U(p, p)$	$\tilde{U} = U(d, d) - U(d, p)$	$\tilde{U} - U$
MnO ₂	12.24	5.67	9.96	6.57	0.36
MnO ₂ /Ir(100)	4.66	1.37	4.34	3.29	-0.49
FeO ₂	15.19	6.13	10.64	9.06	1.39
CoO ₂	14.84	6.22	11.08	8.62	2.89
NiO ₂ (C1)	14.61	6.15	11.26	8.45	1.86
NiO ₂ (C2)	10.31	3.28	8.77	7.03	4.62
NiO ₂ /Ir(100)	1.99	0.83	1.26	1.16	-0.55

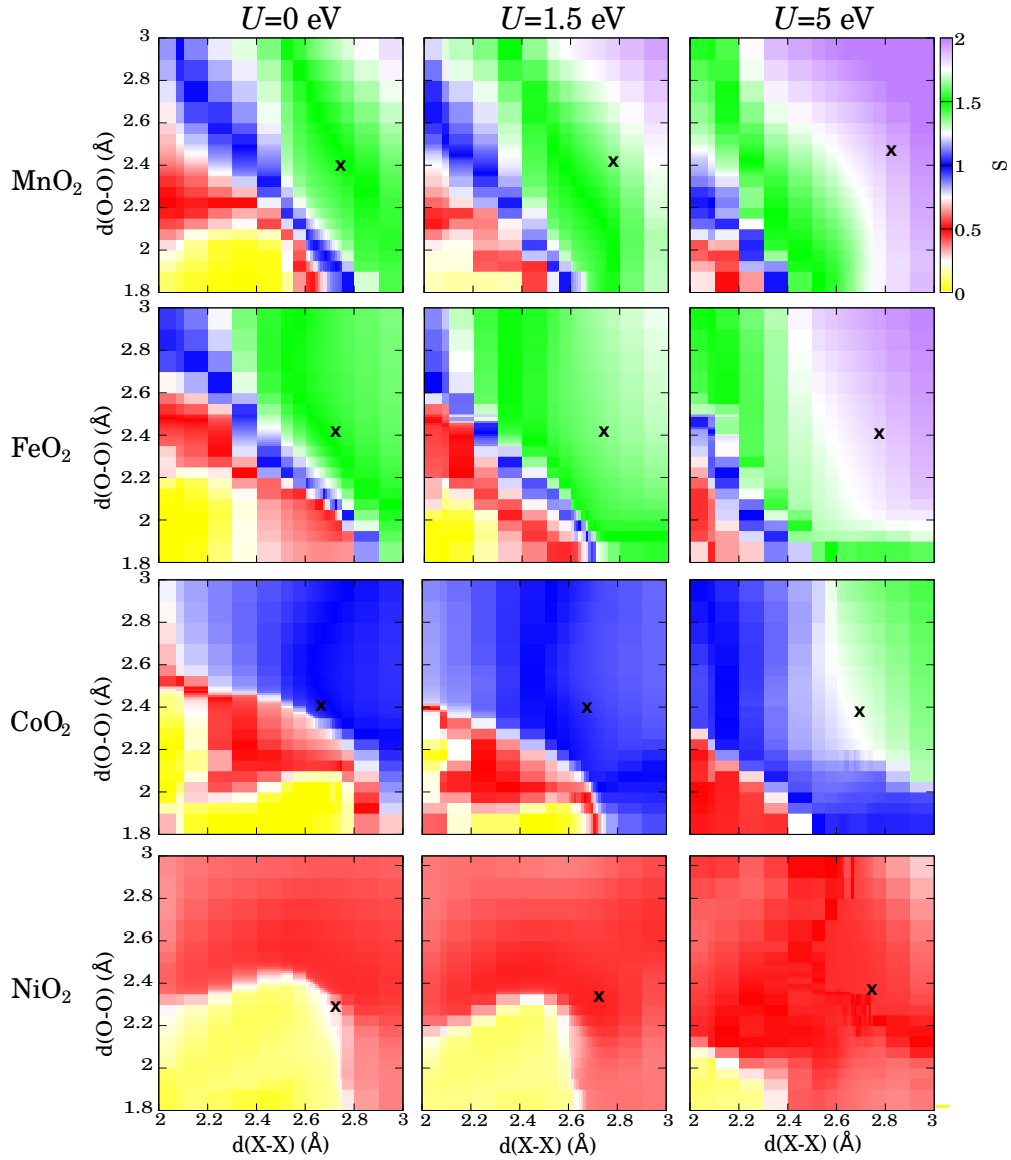


FIG. S1. **Spin states of X in the isolated XO_2 chains.** In these phase diagrams, the color code shows the spin values of the X atom, S , in isolated coplanar XO_2 obtained by calculations with VASP (see caption of Table S1). Each column of panels corresponds to a value of the U parameter and each row to a different X atom. In each panel, the X-O and X-X interatomic distances are varied and the cross indicates the ground state geometry for that U value. Note that U has little influence on the equilibrium geometry. As U increases, except for Ni, the spin can change to a higher value. In addition, more spin states would become accessible by geometry distortion. The regions shaded in white correspond to the transitions between spin states.

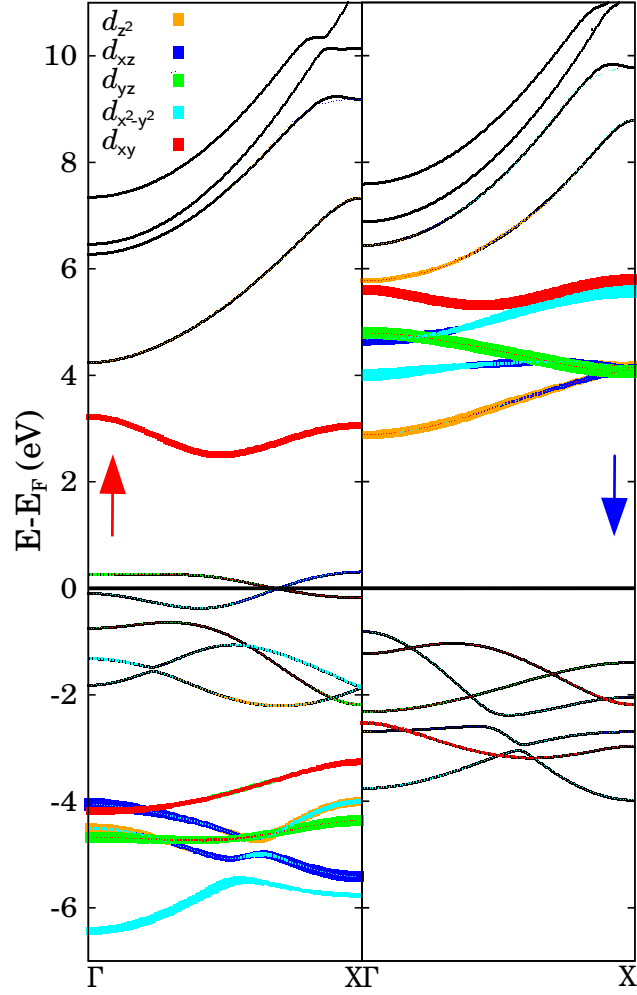


FIG. S2. **Band structure of buckled free-standing MnO₂ chains.** Band structure for free-standing MnO₂ in the buckled geometry adopted during adsorption on the Ir(100) troughs. Left-hand and right-hand panels correspond to majority and minority spin polarization, respectively. The TM's orbital d -characters, indicated in the colour code, are obtained from the corresponding MLWFs, with dot sizes representing the projection magnitudes.

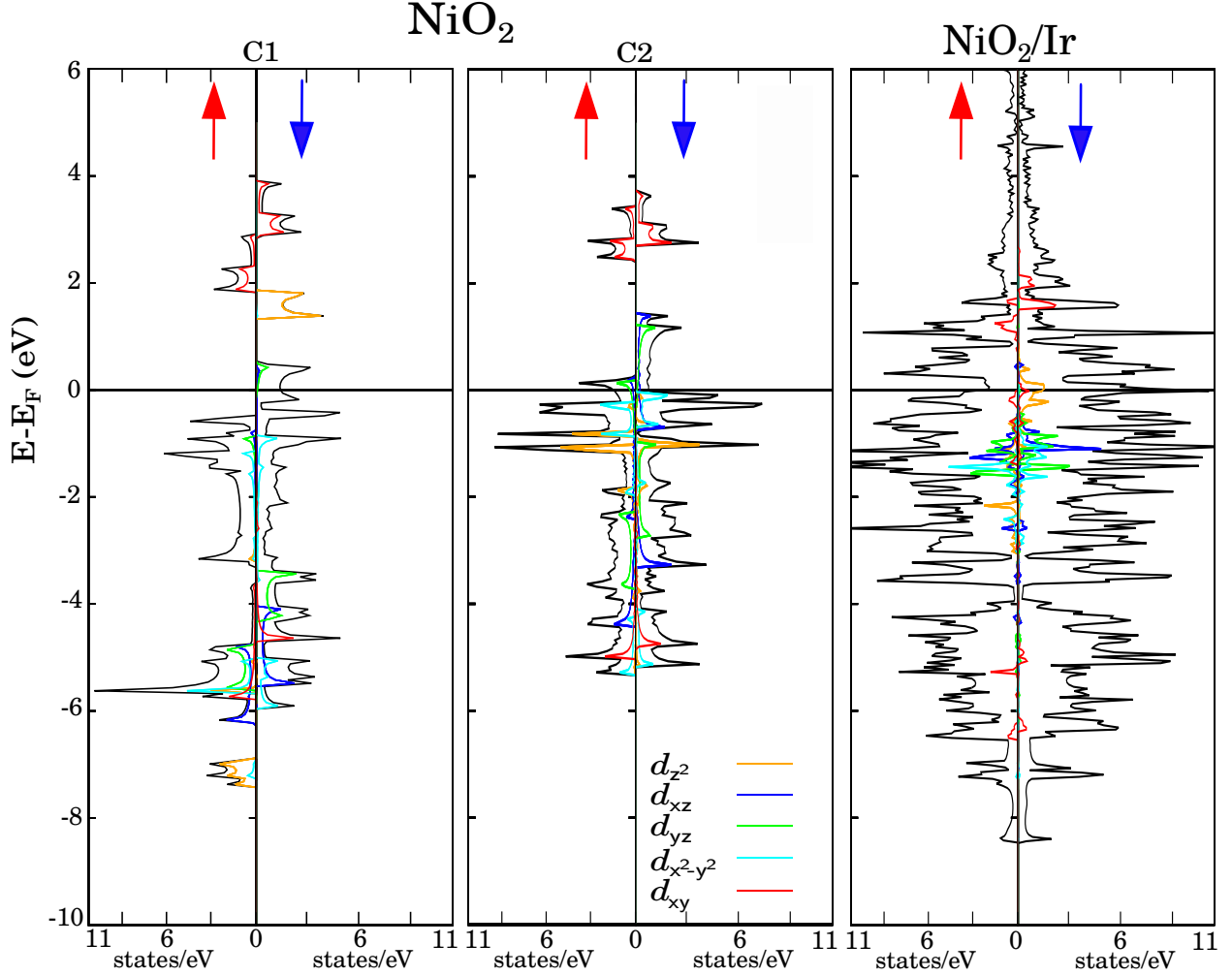


FIG. S3. **Projected densities of states (PDOS) for NiO₂ chains.** In arbitrary units, PDOS of the NiO₂ chains resolved in orbital (colored curves) and spin majority and minority contributions (panels labelled by red and blue arrows, respectively). The black curves account for the total DOS. These PDOS correspond to the band structures shown in Fig. 1 of the main text. The orbital characters are obtained from the corresponding MLWFs. The free-standing planar NiO₂ chain PDOS in the C1 and C2 configurations is shown in the left and middle panels, respectively and the right-hand panel shows the Ir-supported case, where the large substrate contribution is contained in the black curve.

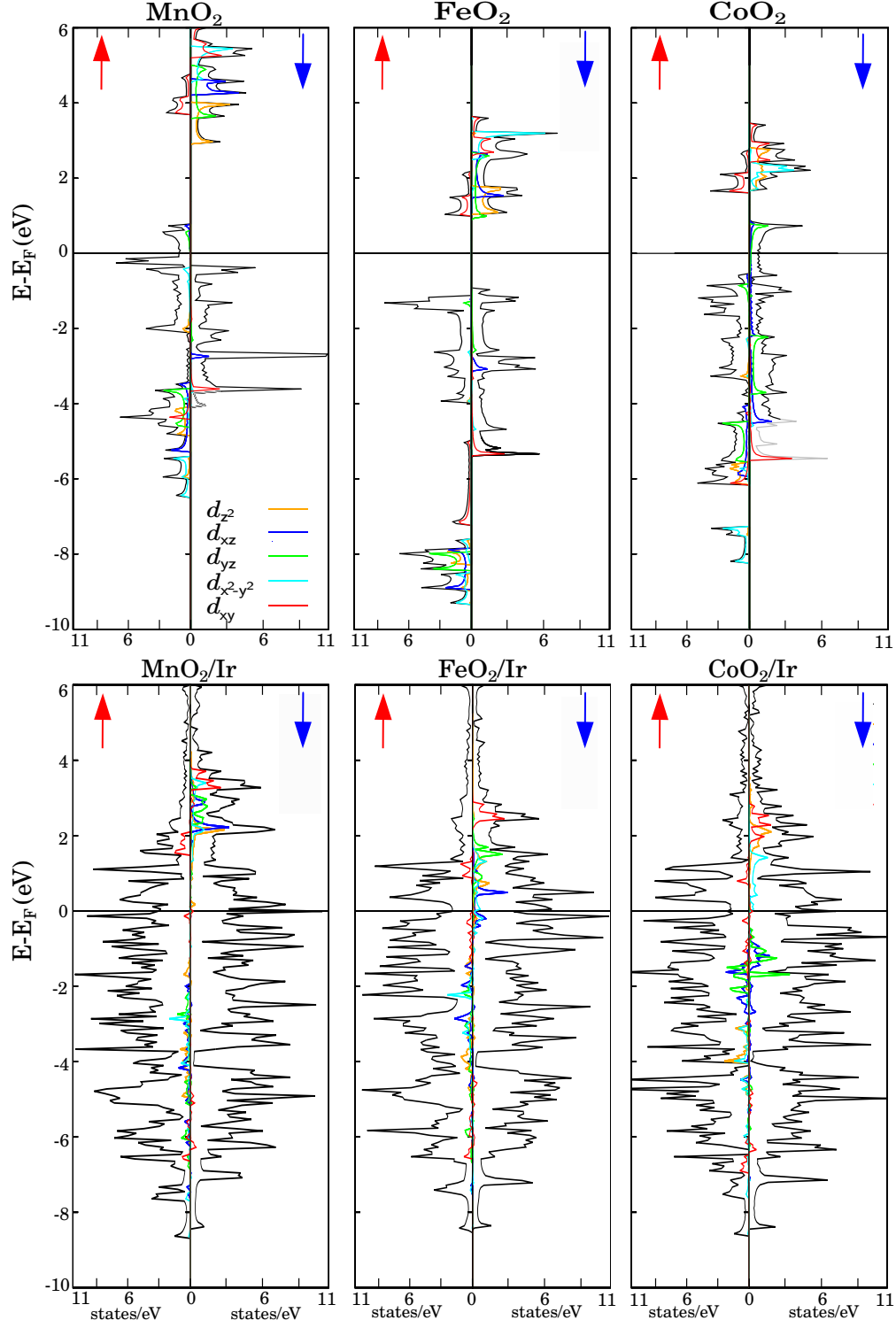


FIG. S4. PDOS for MnO_2 , FeO_2 and CoO_2 chains. The same information as in Fig. S3 (corresponding to the band structures shown in Fig. 3 of the main text) is provided here for free-standing planar (top panels) and supported (bottom panels) XO_2 ($\text{X}=\text{Mn,Fe,Co}$) chains.

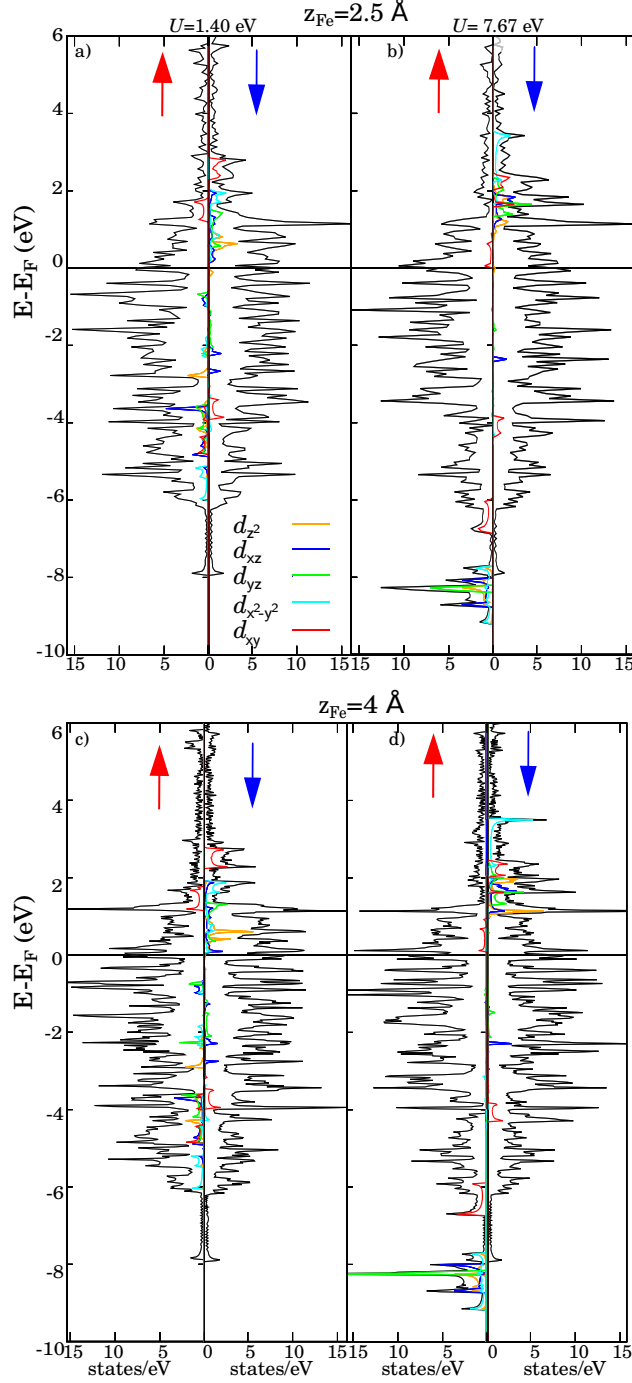


FIG. S5. **Adsorption height dependence of the PDOS for $\text{FeO}_2/\text{Ir}(100)$.** The colored curves show Fe(d) orbital contributions to the PDOS of FeO_2 detached from the Ir(100) substrate at heights 2.5 Å (a,b) and 4 Å (c,d), for $U = 1.40$ and 7.67 eV, which correspond to the limit U values in the adsorbed (a,c) and free standing (b,d) configurations, respectively. The black curve corresponds to the total density of states.

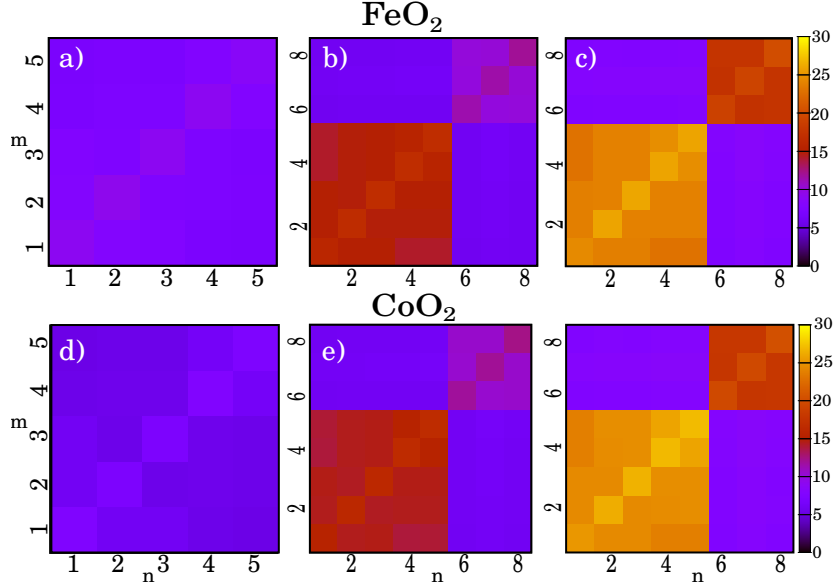


FIG. S6. **Coulomb matrix elements for FeO_2 and CoO_2 isolated chains.** (a,d) Effective U_{mn} elements of the $X(d)$ orbital screened by the rest of electrons. (b,e) U_{mn} of $X(d)$ and $O(p)$ orbitals screened by the rest of electrons (s). (c,f) Bare Coulomb matrix elements U_{mn} for $X(d)$ and $O(p)$ in the isolated XO_2 chains, with $X=\text{Fe}$ (top) and Co (bottom). Indices are ordered as $1 - d_{z^2}$, $2 - d_{xz}$, $3 - d_{yz}$, $4 - d_{x^2-y^2}$, $5 - d_{xy}$, $6 - p_z$, $7 - p_x$ and $8 - p_y$.

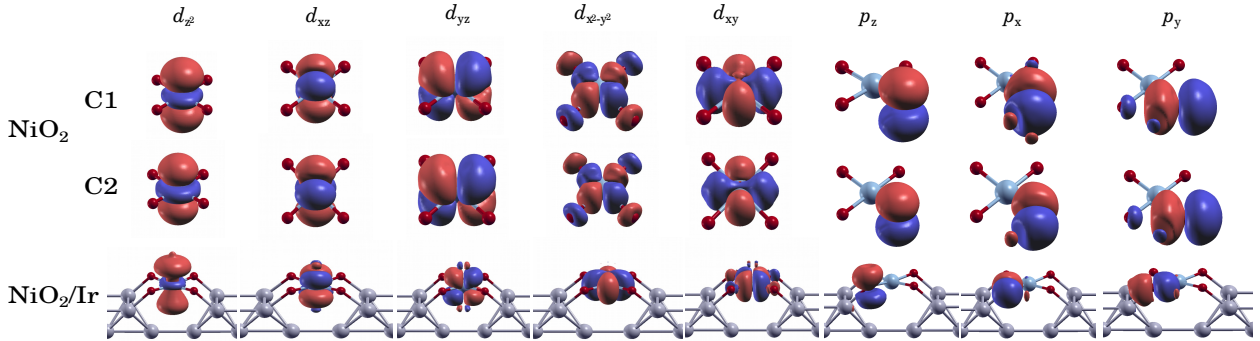


FIG. S7. **Maximally localized Wannier Functions (MLWF) of NiO_2 chains.** Real-space representation of the MLWFs with $\text{Ni}(d, \downarrow)$ and $\text{O}(p, \downarrow)$ character obtained from the spin-minority electronic wavefunctions of free-standing (top row) and Ir-supported (bottom row) NiO_2 . Both electronic configurations of the unsupported chain are included.

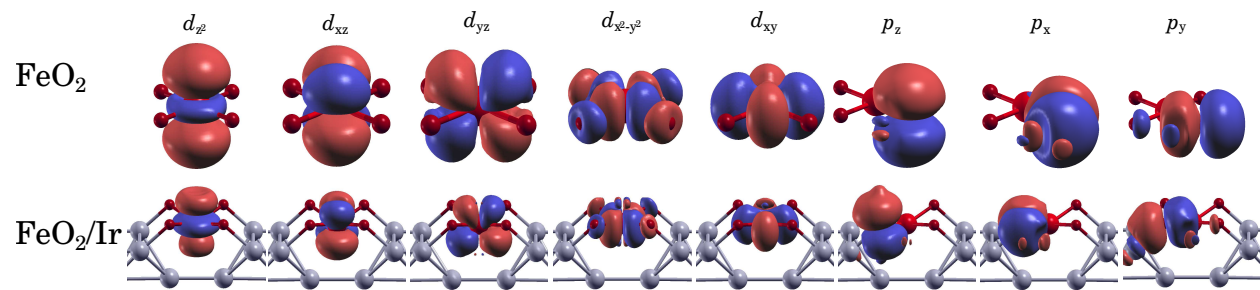


FIG. S8. MLWFs of FeO_2 chains. Same information as in Fig. S7 for the FeO_2 case.

-
- [1] G. Kresse and J. Hafner, Phys. Rev. B **47**, 558 (1993).
 - [2] G. Kresse and D. Joubert, Phys. Rev. B **59**, 1758 (1999).
 - [3] V. I. Anisimov, F. Aryasetiawan, and A. I. Lichtenstein, Journal of Physics: Condensed Matter **9**, 767 (1997).
 - [4] J. P. Perdew, K. Burke, and M. Ernzerhof, Phys. Rev. Lett. **77**, 3865 (1996).
 - [5] H. Krakauer, M. Posternak, and A. J. Freeman, Phys. Rev. B **19**, 1706 (1979).
 - [6] E. Wimmer, H. Krakauer, M. Weinert, and A. J. Freeman, Phys. Rev. B **24**, 864 (1981).
 - [7] A. B. Shick, A. I. Liechtenstein, and W. E. Pickett, Phys. Rev. B **60**, 10763 (1999).
 - [8] FLEUR site: <http://www.flapw.de>.
 - [9] P. Seth, P. Hansmann, A. van Roekeghem, L. Vaugier, and S. Biermann, Phys. Rev. Lett. **119**, 056401 (2017).